CRAGE-mediated insertion of fluorescent chromosomal markers for accurate and scalable measurement of co-culture dynamics in *Escherichia coli*

Avery J.C. Noonan[1], Yilin Qiu[1], Joe C.H. Ho [2], Jewel Ocampo [2], K.A. Vreugdenhil[1], R. Alexander Marr[1], Zhiying Zhao[3], Yasuo Yoshikuni[3,4,5,6,7], and Steven J. Hallam[1,2,8,9,10,11,*]

[1]Genome Science and Technology Program, University of British Columbia, Vancouver, BC V6T 1Z4, Canada, [2]Department of Microbiology & Immunology, University of British Columbia, Vancouver, BC V6T 1Z3, Canada, [3]US Department of Energy Joint Genome Institute, Lawrence Berkeley National Laboratory, Berkeley, CA, USA, [4]Environmental Genomics and Systems Biology Division, Lawrence Berkeley National Laboratory, Berkeley, CA, USA, [5]Biological Systems and Engineering Division, Lawrence Berkeley National Laboratory, Berkeley, CA, USA, [6]Center for Advanced Bioenergy and Bioproducts Innovation, Urbana, IL, USA, [7]Global Institution for Collaborative Research and Education, Hokkaido University, Hokkaido, Japan, [8]Graduate Program in Bioinformatics, University of British Columbia, Vancouver, BC V6T 1Z4, Canada, [9]Biofactorial High-Throughput Biology Facility, University of British Columbia, Vancouver, BC V6T 1Z3, Canada, [10]Life Sciences Institute, University of British Columbia, Vancouver, BC V6T 1Z3, Canada and [11]ECOSCOPE Training Program, University of British Columbia, Vancouver, BC V6T 1Z3, Canada

*Corresponding author: E-mail: shallam@mail.ubc.ca

Abstract

Monitoring population dynamics in co-culture is necessary in engineering microbial consortia involved in distributed metabolic processes or biosensing applications. However, it remains difficult to measure strain-specific growth dynamics in high-throughput formats. This is especially vexing in plate-based functional screens leveraging whole-cell biosensors to detect specific metabolic signals. Here, we develop an experimental high-throughput co-culture system to measure and model the relationship between fluorescence and cell abundance, combining chassis-independent recombinase-assisted genome engineering (CRAGE) and whole-cell biosensing with a P_{emrR}-green fluorescent protein (GFP) monoaromatic reporter used in plate-based functional screening. CRAGE was used to construct *Escherichia coli* EPI300 strains constitutively expressing red fluorescent protein (RFP) and the relationship between RFP expression and optical density (OD_{600}) was determined throughout the EPI300 growth cycle. A linear equation describing the increase of normalized RFP fluorescence during deceleration phase was derived and used to predict biosensor strain dynamics in co-culture. Measured and predicted values were compared using flow cytometric detection methods. Induction of the biosensor lead to increased GFP fluorescence normalized to biosensor cell abundance, as expected, but a significant decrease in relative abundance of the biosensor strain in co-culture and a decrease in bulk GFP fluorescence. Taken together, these results highlight sensitivity of population dynamics to variations in metabolic activity in co-culture and the potential effect of these dynamics on the performance of functional

screens in plate-based formats. The engineered strains and model used to evaluate these dynamics provide a framework for optimizing growth of synthetic co-cultures used in screening, testing and pathway engineering applications.

1. Introduction

The engineering and stable maintenance of synthetic microbial consortia promises to emulate the efficiency, resilience and robustness of microbial community metabolism found in nature (1–4). Recent applications of this paradigm include the distribution of pathways that are energetically costly or depend on host-specific metabolisms from multiple strains to produce increasingly complex biosynthetic outcomes, including the distribution of pathways for production of resveratrol (5) and flavonoids (6, 7). In addition to metabolic engineering applications, the use of whole-cell biosensor strains to report on biochemical changes in co-culture has enabled development of functional screens for enzyme discovery (8–10) and diagnostic tests used to detect the presence of specific metabolites or compounds (11, 12).

Process stability within engineered microbial consortia is sensitive to population dynamics between strains, as these parameters influence the proportion of cells mediating each step in a distributed metabolic pathway or reporting on specific biochemical transformations (13–19). Significant effort has gone into the design and testing of regulatory circuits and cell–cell communication networks that allow control of population dynamics and metabolic activity in co-culture (4, 16, 20–25). These systems enable interrogation of the effects of stochastic gene expression and of social interactions driving functional outcomes at the individual and population levels of organization, resulting in the development of many standardized genetic parts (4). Despite the emerging synthetic biology repertoire, challenges remain in monitoring population and community level dynamics in high-throughput, with implications for whole-cell biosensor performance in screening and diagnostic testing (3, 18, 26, 27).

In monoculture, measuring optical density at 600 nm (OD_{600}) is a standard method of analyzing cell culture density, growth rate and stage (28). Although this proxy is not without inherent bias, given a fixed pathlength, it is possible to approximate total cell number per unit volume of a monoculture (28–30). However, this method cannot distinguish strains in co-culture, providing only a measure of total cell density. Currently, *ex situ* methods such as microscope cell counting, flow cytometry, plating and counting with or without selection, and DNA barcoding are used to investigate population dynamics in co-culture experiments (3, 26, 27). Because these methods do not lend themselves to continuous measurements of strain abundance across co-culture stages, they have limited application to plate-based growth experiments. This restricts the application of high-throughput methods that require accurate monitoring of population dynamics, including the use of whole-cell biosensors in co-culture.

Here, we develop an experimental high-throughput co-culture system in which to measure and model the relationship between fluorescence and total cell abundance, combining chassis-independent recombinase-assisted genome engineering (CRAGE) (31) and whole-cell biosensing with a P_{emrR}-green fluorescent protein (GFP) monoaromatic reporter used in plate-based functional screening (8).

2. Materials and methods

2.1 Plasmids and strains

Functional screening host *Escherichia coli* EPI300 [F⁻ λ⁻ *mcrA* Δ(*mrr-hsdRMS-mcrBC*) Φ80d*lacZ*ΔM15 Δ(*lac*)X74 *recA1 endA1 araD139* Δ(*ara, leu*)7697 *galU galK rpsL* (Str^R) *nupG' trfA dhfr*] (EPI300) (Lucigen) was used in all culturing experiments. Conjugal donor strain *E. coli* WM3064 (*thrB1004 pro thi rpsL hsdS lacZ*ΔM15 RP4-1360 Δ(*araBAD*)567 Δ*dapA1341::[erm pir]*) (32) was used in strain engineering employing the CRAGE system. Biosensor plasmids were constructed with the pSB1C3 and pET-15b vectors. CRAGE engineering required modification of pCC1-KMW2-SpCre-3L (33) and pW34 plasmids. For more information on the plasmids and strains used, consult the Supplementary Materials.

2.2 CRAGE system establishment

The CRAGE landing pad was amplified from the pCC1-KMW2-SpCre-3L plasmid (33) using primers 3lox_Tn5_F and 3lox_Tn5_R, which generates amplicons flanked with 19 bp inverted repeats necessary for Tn5 transposition (34). The landing pad was then integrated into the chromosome of the functional screening host *E. coli* EPI300, using the EZ-Tn5 Transposase kit (Lucigen), generating the EPI300-CRAGE strain. Chromosomal DNA was extracted from EPI300-CRAGE using a CTAB extraction and digested with NraIII (NEB), generating fragments with a known portion of the landing pad adjacent to an unknown segment of the chromosome. Digested chromosome was then self-ligated with T4 DNA ligase (NEB), producing primarily circularized DNA composed of a single digested fragment. Outward facing primers SBP4940_F and SBP7924_R were used to amplify the non-landing-pad portion of the circularized fragment. The chromosomal integration of the CRAGE landing pad was confirmed, and its location identified based on Sanger sequencing of the genomic interval adjacent to the landing pad integration site. For more information on the primers and constructs used, consult the Supplementary Materials.

2.3 Biosensor strain engineering

Four constructs containing red fluorescent protein (RFP, BBa_E1010) under the control of synthetic *E. coli* promoters from the J23100 promoter series (BBa_J23100, BBa_J23106, BBa_J23113 and BBa_J23114) were assembled in the pSB1C3 vector using the standard International Genetically Engineered Machine (iGEM) BioBrick assembly protocol (35, 36). BioBrick-agnostic primers containing flanking regions homologous to the pW34 vector backbone were designed to amplify the RFP constructs for Gibson assembly into pW34 using the Hi-Fi Gibson Assembly Master Mix (NEB). The pW34 vector backbone was amplified using pW34_AN_F and pW34_AN_R primers, producing amplicons with 30 bp of complementarity to the amplified J23100-series-RFP constructs. Four modified pW34 plasmids were constructed containing the four J23100-series-RFP constructs described above. These were transformed into chemically competent WM3064 conjugal donor strain and plated on LB agar plates

(50 µg ml^{-1} apramycin and 57 µg l^{-1} DAP). After 24 h at 37°C, the colonies were inoculated into 200 µl culture in 96-well microplate format and incubated for 16 h. OD$_{600}$ of culture was then measured using a Varioskan Flash plate reader (Thermo Fisher Scientific) and the five donor strains were incubated with the EPI300-CRAGE recipient strain at a 4:1 ratio, based on OD$_{600}$ measurements. After 4 h of incubation, conjugation product was streaked on 50 µg ml^{-1} apramycin LB agar plates without DAP to select for uptake of the pW34 plasmid. Chromosomal integration into the CRAGE landing pad was determined based on Sanger sequencing.

2.4 Culturing and measurements

All culture experiments were performed in 384-well black clear bottom plates (Nunc), at 85 µl volume in LB and one or more antibiotics as appropriate: chloramphenicol (12.5 µg ml^{-1}), apramycin (100 µg ml^{-1}), ampicillin (100 µg ml^{-1}) or kanamycin (50 µg ml^{-1}). Cultures were inoculated using an Echo 525 liquid handling system (Labcyte) or QPix2 automatic colony picking robot (Molecular Devices), and media was dispensed using a MultiFlo (BioTek) or Multidrop Combi reagent dispenser (Thermo Scientific). Plates were incubated at 37°C in a Cytomat C5 series automated incubator (Thermo Scientific) and transferred to a PHERAstar plate reader (BMG) within an integrated Access workstation (Labcyte) for measurements every hour during measurement cycles. Plates were shaken for 20 s in the PHERAstar prior to taking optical density measurements at 600 nm (OD$_{600}$). Fluorescence readings were taken from the top at excitation/emission wavelengths of 485/520 nm (GFP) and 575/610 nm (RFP), respectively. Unless otherwise noted, all conditions, including strain types, inoculation ratios and induction concentrations, were inoculated in triplicate.

2.5 Flow cytometry

Cells were resuspended and diluted in filter sterilized M9 media to approximately 20 000 cells in a 200 µl volume. Cells were then stained with 4′,6-diamidino-2-phenylindole (DAPI) ([37]) to differentiate cells from debris in the media. Cells were counted using the Attune NxT Acoustic Focusing Cytometer (Invitrogen). A blue laser (488 nm), yellow laser (561 nm), violet laser (405 nm) and red laser (637 nm) allowed analysis of variability in GFP fluorescence, RFP fluorescence, DAPI fluorescence, side scatter and forward scatter. At least 15 000 cells were counted per sample and populations in co-culture were determined based on these results. Strain-specific OD$_{600}$ values were calculated by multiplying strain proportions by bulk OD$_{600}$ values.

2.6 Data analysis

PHERAstar plate reader (BMG) output was imported and consolidated using an in-house Python script. The resulting data frame was then processed and analyzed in the statistical computing environment R. Data transformations, as well as errors and models were calculated in R using built-in functions and R packages from the Tidyverse collection ([38], [39]). Associated R scripts and data are included in Supplementary Materials.

2.7 Plasmid availability

Plasmid availability is included in Supplementary Materials.

3. Results and discussion

In previous studies, P$_{emrR}$-GFP biosensor activity was correlated to a range of vanillin and syringaldehyde concentrations and was adapted as a screening tool for lignin transformation phenotypes in co-culture with *E. coli* EPI300 clones harboring large insert (fosmid) DNA (Supplementary Figure S1A) ([8]). The level of GFP expression by the P$_{emrR}$-GFP biosensor strain was assumed to be proportional to the concentration of monoaromatics generated by fosmid clone activity under uniform co-culture conditions. However, as screening throughput increased, it became evident that variation in cell densities across 384-well plates (2.5-fold variation between maximum and minimum OD$_{600}$ values) had the potential to increase false discovery due to fitness trade-offs, residual GFP expression and the inability to generate a normalized or relative GFP fluorescence across all co-cultures (Supplementary Figure S1B). To better monitor these dynamics, CRAGE was used to insert a single copy of a constitutively expressed RFP in the chromosome of the P$_{emrR}$-GFP biosensor strain, enabling simultaneous measurement of GFP and RFP. Given the cell-to-cell variability in copy number and gene expression under plasmid control, the *RFP* cassette was inserted into the chromosome as opposed to being maintained by a plasmid. Resulting fluorescence ratios were then used to model cell density of the biosensor strain in co-culture at different growth stages and vanillin concentrations to facilitate more accurate screening outcomes in plate-based formats.

3.1 Biosensor strain engineering with CRAGE

The CRAGE system enables high-efficiency *Cre-lox*-mediated integration of genes or gene cassettes across diverse taxonomic lineages at the site of a chromosomal landing-pad ([31]). This allows the integration of gene cassettes or clusters of up to 100 kilobases (Figure 1B). To facilitate studies of biosensor-based co-culture dynamics, CRAGE was established in the functional screening strain *E. coli* EPI300 (EPI300), through transposition-mediated integration of the CRAGE landing-pad, generating the EPI300-CRAGE strain (Figure 1A). Sanger sequencing indicated that the landing pad was inserted into the *yfaA* locus, predicted to encode a domain of unknown function, DUF2300 (Figure 1B).

Constitutive *RFP* gene cassettes, consisting of a promoter from the J23100 synthetic promoter series driving *RFP* expression, were integrated into the landing-pad through conjugation of modified pW34 plasmids from the conjugal donor strain WM3064 and subsequent recombination into the EPI300-CRAGE chromosome. Observed RFP expression levels from constitutive promoters of the J23100 synthetic promoter series were consistent with previous reports ([40]), with promoters J23100 and J23106 providing the highest single copy expression levels (Figure 1C). Growth experiments with the CRAGE-J23100 and CRAGE-J23106 strains confirmed the non-essentiality of *yfaA*, with minimal fitness effects when grown in LB media compared to the unmarked EPI300 parental strain (Figure 1D). The pSB1C3-P$_{emrR}$-GFP biosensor plasmid was subsequently transformed into EPI300-CRAGE harboring either the J23100-RFP or J23106-RFP constructs, producing RFP marked biosensor strains J23100 and J23106, capable of monoaromatic-dependent GFP expression (Figure 1A).

3.2 Strain characteristics in monoculture

The growth and biosensor-response patterns of the J23100 and J23106 biosensor strains were evaluated to determine the
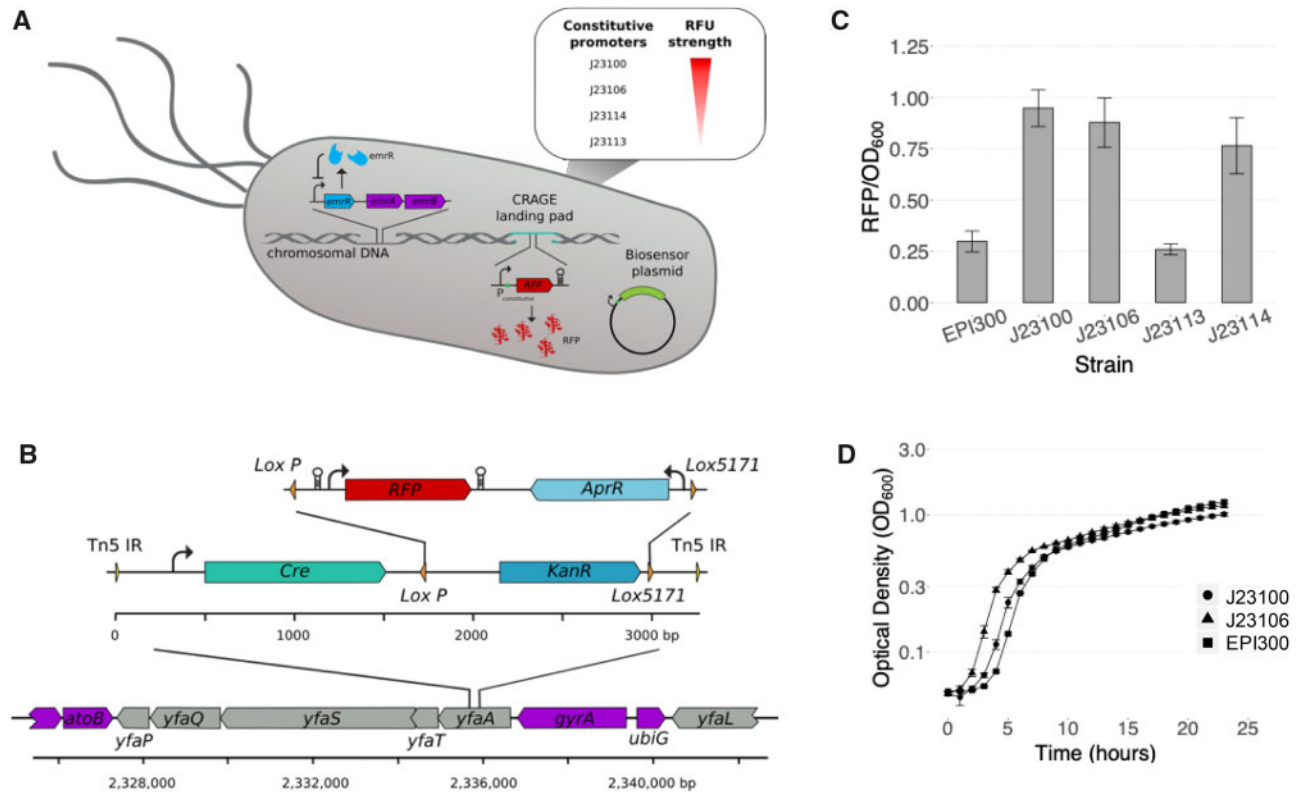
Figure 1. CRAGE-enabled engineering of *E. coli* EPI300 reporter strains. (**A**) The emrR transcriptional regulator enables monoaromatic-dependent GFP expression following transformation with the pSB1C3-P_{emrR}-GFP biosensor plasmid. Four constitutive RFP expression cassettes, with a range of promoter strengths, were integrated into the chromosome as a method of labeling the reporter strain. (**B**) Chromosomal integration was performed using the CRAGE system, requiring landing pad transposition into the EPI300 chromosome. This enables high-efficiency *Cre-lox*-recombination into the CRAGE landing pad site. The location of integration was determined to be the *yfaA* gene. (**C**) RFP fluorescence/OD_{600} (*Normalized RFP*) was calculated for the J23100, J23106, J23113 and J23114 strains after 24 h of incubation. Columns represent averages of two replicates. (**D**) OD_{600} of CRAGE-engineered strains (J23100 and J23106) and EPI300 were monitored over 24 h (*Time*). OD_{600} values represent averages of three replicates.

relationship between fluorescence and cell abundance under inducing conditions. In order to simplify presentation of results, all figures describing the J23106 biosensor strain can be found in the Supplementary Materials. Initially, optical densities of J23100 and J23106 were observed over 24 h at various vanillin induction concentrations to determine the impact of constitutive RFP and induced GFP expression on growth rates (Figure 2B/Supplementary Figure S2B for J23106). No significant difference was observed between growth curves of the biosensor strains, at different vanillin induction levels. All strains entered exponential phase between 5 and 6 h after induction and entered a deceleration phase around 12 h after induction, at an OD_{600} of 0.6–0.7 (Figure 2B/Supplementary Figure S2B for J23106). This extended deceleration phase prior to entry into stationary phase is well documented and has been observed in both microplate and flask-based growth experiments (28, 41).

Moreover, monoaromatic-inducible expression of GFP from the pSB1C3 plasmid and the constitutive expression of RFP from the chromosome were entirely independent of one another (Figure 2C and D/Supplementary Figure S2C and D for J23106) indicating that RFP fluorescence remains proportional to the abundance of biosensor-containing cells, regardless of the induction level of GFP. Taken together, these results indicate that the J23100 and J23106 biosensor strains grown in monoculture are on par with the original P_{emrR}-GFP strain and that constitutive RFP expression in both strains has no impact on the induction response of the reporter plasmid.

3.3 Proportionality of RFP expression and optical density

After evaluating the stability of FP fluorescence in the J23100 and J23106 biosensor strains, the relationship between RFP fluorescence and optical density was determined at different growth stages. Although OD_{600} measurements are primarily indicative of light scattering resulting from culture turbidity, the relationship between OD_{600} and cell number can be influenced by medium composition and absolute culture density. Despite this resulting in decreased sensitivity at low and high culture densities, ease and non-invasiveness of measurements, as well as functional equivalency have led to widespread application of OD_{600} measurements as a proxy for cell abundance (28–30, 41). As background fluorescence is significantly higher than background OD_{600} measurements in 384-well format, we observed that the ratio of RFP fluorescence and optical density decreased from the time of inoculation until the optical density reached a critical point (Figure 3A). This observation results from the fact that increases in OD_{600} above background of approximately 0.05 can be observed as early as 3 h post-inoculation, whereas increases in RFP fluorescence above background of approximately 9500 RFU are only observed as early as 9 h after inoculation, at which point OD_{600} values have increased approximately 10-fold above background (Figure 3A/Supplementary Figure S3A for J23106). This trend can be related to specific stages in the *E. coli* growth cycle, with the highest RFU/OD_{600} values during lag-phase (0–5 h), resulting from the low denominator, a rapid decrease in RFU/OD_{600} values during exponential-phase
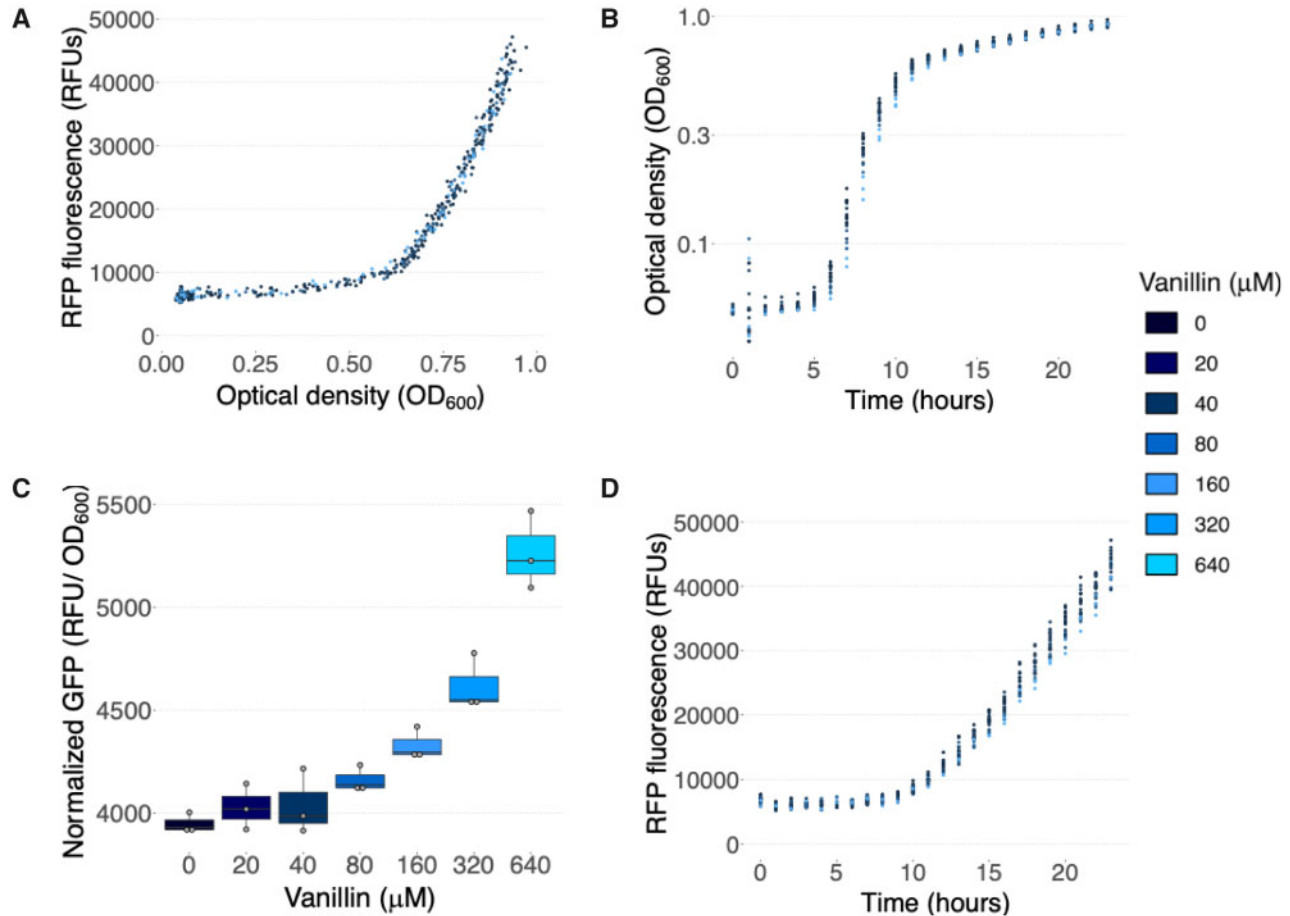
Figure 2. Biosensor strain growth characteristics and response in monoculture. (**A**) In J23100 biosensor strain, with chromosomally integrated constitutively expressed RFP constructs, there is a non-linear relationship between RFUs (*RFP fluorescence*) and OD_{600} (*Optical density*). Values represent single samples in 384-well format at various vanillin induction concentrations. (**B**) OD_{600} (*Optical density*) values were measured hourly for 24 h (*Time*), at 7 vanillin concentration ranging from 0 to 640 µM, to observe the impact of vanillin induction on growth rate of biosensor strains. Biosensor response was observed in RFP-labeled strains to determine the impact of co-expression of vanillin-induced GFP and constitutively expressed RFP. OD_{600} values represent single samples in 384-well format at various vanillin induction concentrations. (**C**) The response of the P_{emrR}-GFP biosensor (*Normalized GFP*) to vanillin induction at 7 concentrations (*Vanillin*) is shown at 14 h after inoculation of the J23100 strain. Boxes were set using three single sample replicates in 384-well format. (**D**) RFP fluorescence in RFUs in the J23100 strain over 24 h (*Time*), at 7 vanillin induction concentrations. RFP fluorescence values represent single samples in 384-well format at various vanillin induction concentrations.

(5–11 h), resulting from the rapid increase in OD_{600} without a significant increase in RFUs, followed by a consistent and near linear increase in RFU/OD_{600} values during deceleration phase (Figure 3B/Supplementary Figure S3B for J23106). The consistency of the pattern of RFP fluorescence in relation to OD_{600} values, and the linear increase of this ratio during the deceleration phase of the *E. coli* growth cycle, which coincides with the increase of RFP fluorescence above background values, provides a framework for modeling the relationship between RFP fluorescence and OD_{600}.

3.4 Modeling the relationship between RFP fluorescence and OD_{600}

Based on the stage-specific relationship between RFU and OD_{600} observed above, a linear model was developed to predict cell abundance based on RFP fluorescence following the transition into deceleration phase at approximately 12 h of growth in 384-well format. This requires the definition of the time of entry into deceleration phase on a single-culture basis. Although the culture density OD_{600} = 0.65 was consistently associated with entry into deceleration phase in monoculture, strain-specific

OD_{600} is not measurable in co-culture, demanding an alternative method of defining this transition. The first derivative of OD_{600}/time indicates the rate of increase in OD_{600}, which will peak in log phase and decrease into deceleration phase. Calculating the rate of change of this value shows a maximum at the entry into log phase, when the growth rate is increasing most rapidly, and a minimum at the entry into deceleration phase, when the growth rate is decreasing most rapidly (Figure 3C/Supplementary Figure S3C for J23106). These values are defined by Equation 1, which allows the OD_{600}-based definition of time of entry into deceleration phase. The double-derivative of the growth curve at a time of t_n is determined by subtracting the change in OD_{600} (OD_n) between t_{n-1} and t_{n-2} from the change in OD_{600} (OD_n) between t_n and t_{n-1}, giving the change in growth rate between t_{n-1} and t_n.

$$\frac{\delta^2 OD}{\delta t^2} = \left(\frac{OD_n - OD_{n-1}}{t_n - t_{n-1}} \right) - \left(\frac{OD_{n-1} - OD_{n-2}}{t_{n-1} - t_{n-2}} \right) \quad (1)$$

$$\frac{\delta RFP}{\delta t} / RFP = \frac{RFP_n - RFP_{n-1}}{t_n - t_{n-1}} / RFP_{n-1} \quad (2)$$
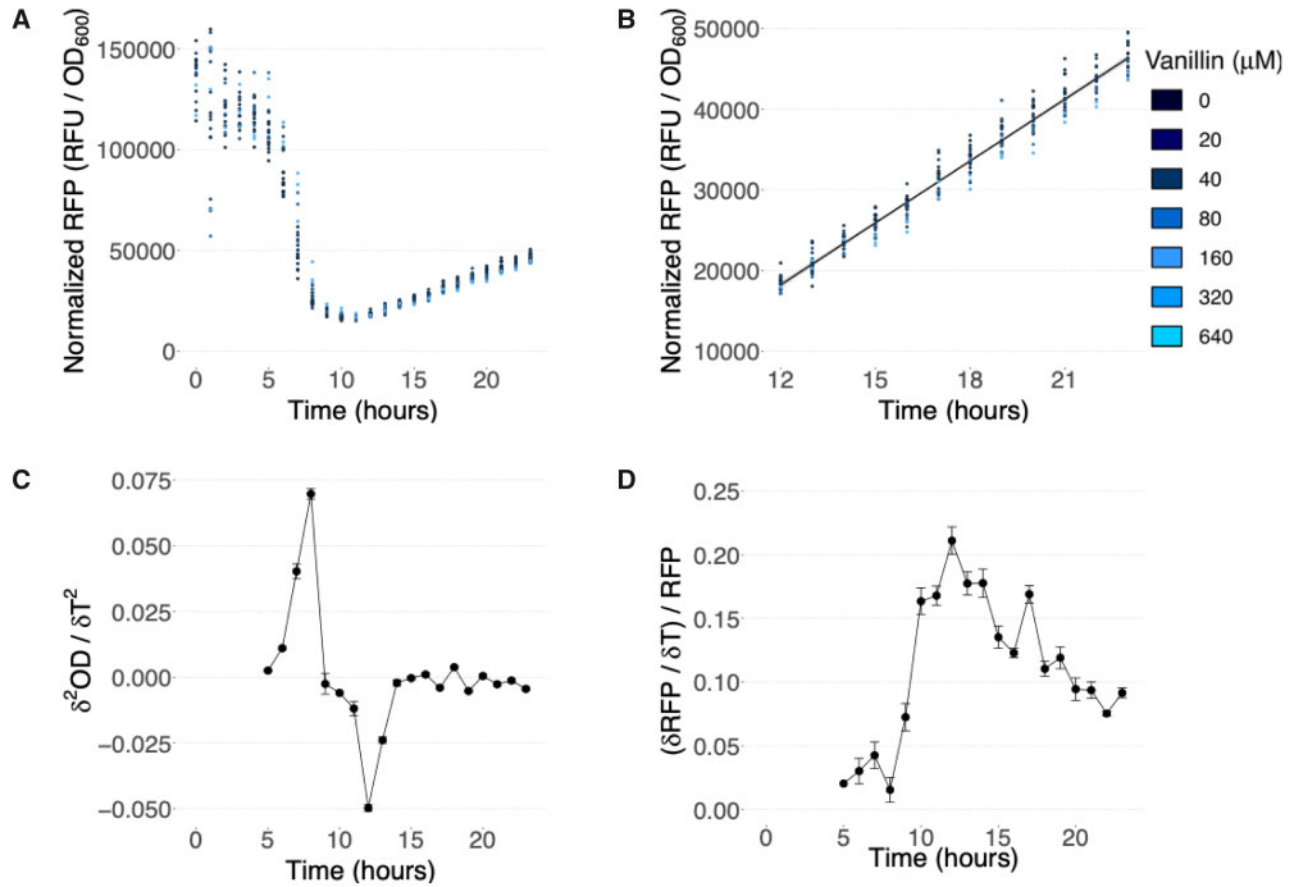
Figure 3. Characterizing the relationship between RFP fluorescence and OD$_{600}$ over the *E. coli* growth cycle. (**A**) The ratio of RFP RFUs/OD$_{600}$ (*Normalized RFP*) plotted over 24 h (*Time*) in strain J23100, at 7 vanillin induction levels, shows the non-linearity of RFP fluorescence/OD$_{600}$. Values represent single samples in 384-well format. (**B**) A linear relationship between RFU/OD$_{600}$ (*Normalized RFP*) and time (*Time*) can be observed during the deceleration phase of the *E. coli* growth cycle. This requires defining T$_0$ of this relationship as the entry into deceleration phase. Points represent single samples in 384-well format at 7 induction concentrations. The linear trend is represented by Equation 3. (**C**) The minimum ($t = 8$) and maximum ($t = 12$) in the double-derivative of the growth curve ($\delta^2 OD/\delta T^2$) of J23100 indicate times (*Time*) of the largest positive and negative rates of change of growth rate. Values represent averages of 21 samples at 7 induction concentrations. (**D**) The relative increase in RFP fluorescence (*Relative δRFP/δT*) over time shows a maximum ($t = 12$) at the time (*Time*) of entry into deceleration phase. Values represent averages of 21 samples at 7 induction concentrations.

In the trend of RFP fluorescence over time the entry into deceleration phase is marked by an increase in the rate of RFP expression, which can be observed by plotting the rate of increase in RFP fluorescence, relative to the total RFUs (Equation 2) (Figure 3D/Supplementary Figure S3D for J23106). The relative rate of RFP increase at a time of t_n is determined by dividing the change in RFP fluorescence (RFP$_n$) from t_n to t_{n-1} by the RFP fluorescence at t_{n-1}, giving the relative increase in RFP fluorescence between t_{n-1} and t_n. The maximum at 12 h coincides with the entry into deceleration-phase as determined through analysis of the growth curve, as well as with the start of the linearity of RFUs/OD$_{600}$ over time. This enables the defining of a T0 independently of OD$_{600}$ values that cannot be determined in a co-culture setting.

With T$_0$ redefined as the entry into deceleration phase, we performed a linear regression in order to construct a model to represent the relationship between RFP fluorescence and optical density over time in strain J23100 (Equation 3/Supplementary Equation S1 for J23106). Residuals indicated that a linear trend is a suitable model of the relationship. In this model, the slope of 2367 is in units of (RFU/OD$_{600}$)/t, representing the variation in normalized RFP fluorescence over time. The Y-intercept of 18 211 is in units of RFU/OD$_{600}$, representing the normalized RFP fluorescence at the time of entry into deceleration-phase. This

model enables the prediction of OD$_{600}$ values, based on RFP fluorescence.

$$\frac{\text{RFP}}{\text{OD}_{600}} = 2367 \times \ t' + 18\ 211 \tag{3}$$

The accuracy of model predictions was verified in monoculture at three inoculation densities (0.5×, 1× and 5× densities used in monoculture experiments) and two vanillin induction concentrations (0 μM and 320 μM). This validation experiment enabled direct comparison of measured and predicted OD$_{600}$ values. As observed in previous experiments, vanillin induction did not impact the relationship between RFP fluorescence and optical density, and the model was able to accurately approximate culture density based on raw RFU values alone (Supplementary Figure S4).

These results indicate that RFP fluorescence can be used to approximate OD$_{600}$ of the J23100 biosensor strain in monoculture at various vanillin induction concentrations. Increased variability in predicted values result from noisiness in the fluorescence measurements. In order to correlate biosensor response to relative abundance of the biosensor strain in coculture, it is necessary to determine the extensibility of the proposed linear model to the J23100 strain when grown with

EPI300 with and without fosmid clones. This would enable us to discern the biosensor proportion of co-cultures on a well-by-well basis, in order to determine relative biosensor response.

3.5 Co-culturing with novel biosensor strains

Given the linearity of the relationship between normalized RFP fluorescence and time in the J23100 and J23106 biosensor strains during deceleration-phase, we investigated the applicability of this model to the prediction of strain-specific OD_{600} values in plate-based co-culture. As a preliminary validation, we inoculated co-cultures including one of the J23100 and J23106 biosensor strains and EPI300 harboring an empty pCC1 vector (EPI300-pCC1) used in the construction of fosmid clone libraries at five different mixing ratios (10%, 25%, 50%, 75% and 90%) induced with three concentrations of vanillin (0 μM, 320 μM and 640 μM). For each mixing ratio and induction concentration, we monitored OD_{600}, RFP fluorescence and GFP fluorescence on a well-by-well basis, enabling the prediction of biosensor strain cell density using the linear model described above.

The overall optical density of co-cultures remained constant, regardless of inoculation ratios or vanillin concentration (Figure 4A and B/Supplementary Figure S5A and B for J23106). We observed an earlier entry into both log and deceleration-phases in comparison to in monoculture experiments. This likely results from inoculation density, which is variability prone, depending on inoculation technique. As overall growth trajectories were similar when T0 timepoints were aligned

(Supplementary Figure S6), this variation should not affect the accuracy of the model if it is to be applied in screening pipelines. At a given vanillin induction concentration, RFP (Figure 4C/Supplementary Figure S5C for J23106) and GFP fluorescence (Figure 4D/Supplementary Figure S5D for J23106) increased proportionately to the ratio of the biosensor inoculated in co-culture. This observation was expected given that the biosensor strain is the only strain in co-culture to express the reporter genes. Interestingly, with increasing vanillin concentrations, we observed decreasing levels of GFP and RFP fluorescence, in contrast to monoculture observations (Figure 4C and D). Previously, RFP fluorescence and OD_{600} values were unaffected by vanillin induction and GFP fluorescence increased with induction of the P_{emrR}-GFP biosensor.

The inverse correlation observed between GFP fluorescence and vanillin concentration in co-culture has implications for the use of this system in whole-cell biosensing. When using GFP expression alone as a proxy for monoaromatic concentration, these results would have indicated the inverse of the expected readout, as well-level GFP fluorescence decreased with increasing vanillin concentrations. Decrease in the relative abundance of the biosensor strain in co-culture is likely due to fitness costs associated with increased GFP expression in response to monoaromatic induction. Modeling population dynamics based on RFP fluorescence may enable the explanation of these deviations from expected trends and more accurate interpretation of biosensor response in co-culture.
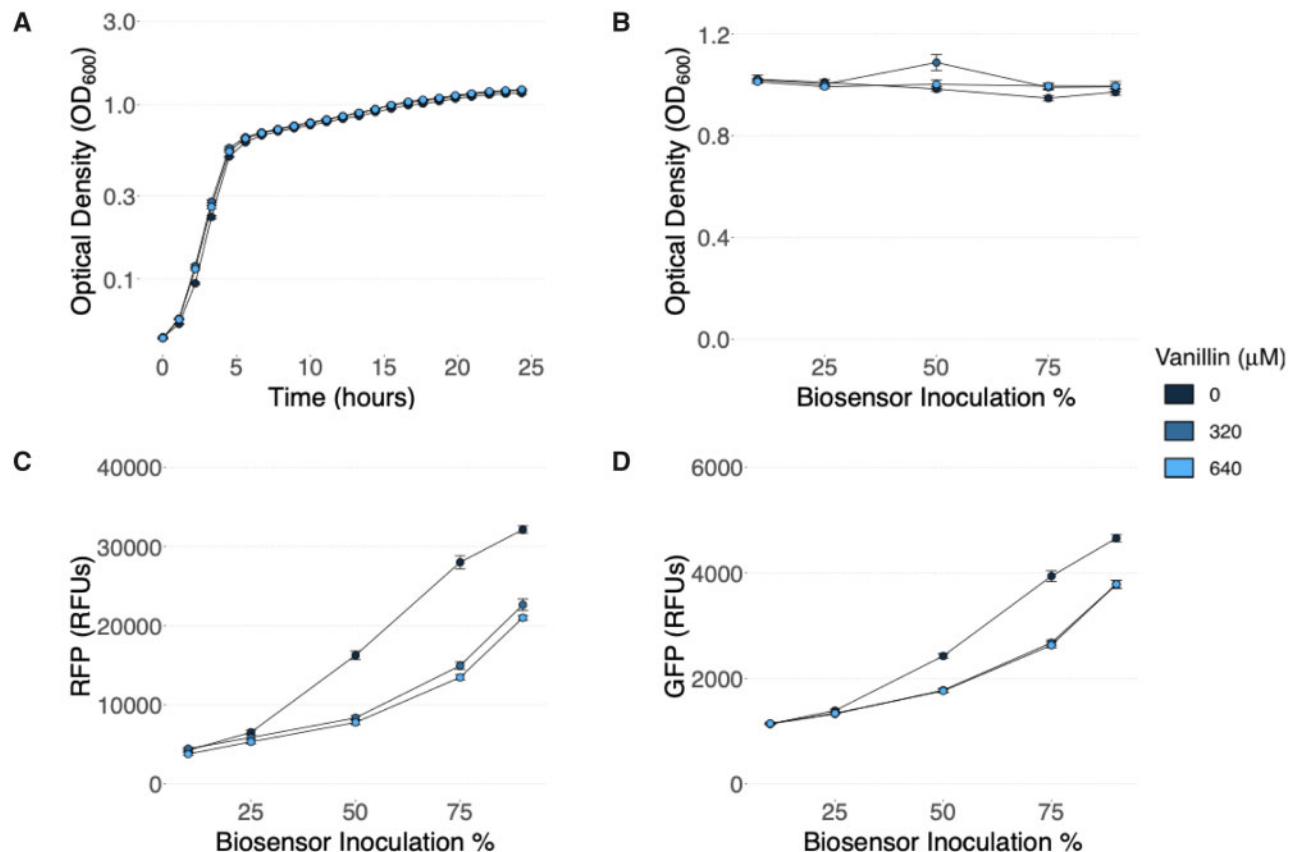

Figure 4. Monitoring bulk co-culture behavior. (**A**) Co-culture-level growth characteristic (*Optical density*) did not differ significantly between vanillin concentration over time (*Time*). (**B**) At a single timepoint (T_{15}), neither inoculation ratio (*Biosensor Inoculation %*) or vanillin induction concentration had a significant impact on measured OD_{600} values (*Optical density*). (**C** and **D**) However, variation in the initial inoculation density of the biosensor strain (*Biosensor Inoculation %*), as well as the concentration of vanillin, both had a significant impact on fluorescence of RFP and GFP (*GFP/RFP*). All values represent averages of three replicates.

3.6 Modeling of biosensor strain OD_{600} in co-culture

As determined through modeling of growth dynamics in mono-culture, approximation of strain-specific OD_{600} in co-culture from RFP fluorescence requires determination of the time of entry into deceleration phase. This point is then redefined as T_0 in the linear model. The previously observed stochasticity of growth-rate and biosensor response requires the T_0 timepoint, as well as relative strain abundance, to be defined on a well-by-well basis. We evaluated the possibility of defining this point either through co-culture level OD_{600} values or strain-specific RFP fluorescence, by calculating the minimum in the double-derivative of the OD_{600} trend or the maximum in the relative $\delta RFP/\delta T$ trend, respectively. Although both methods were indicative of entry into deceleration phase in monoculture, we wanted to determine which values most accurately represented the dynamics of the RFP fluorescence/OD_{600} in co-culture. These methods produced slightly different values of T_0, with more variability in the RFP-dependent calculation at different biosensor mixing ratios (Supplementary Figure S7B and D). T_0 values were defined as 5.6 h, using co-culture level entry into deceleration phase (Supplementary Figure S7A and C) and between 4.5 and 11 h using the maximum relative increase in RFP fluorescence (Supplementary Figure S7B and D).

As T_0 values were relatively consistent between definition methods at higher inoculation ratios, and definition using RFP fluorescence resulted in significantly more variability at lower inoculation ratios, we selected well-level OD_{600} to define T_0. Once defined, this T_0 indicated the start of the linear relationship between RFP/OD_{600} and time. We were then able to approximate strain-specific OD_{600}, as demonstrated in mono-culture, on a well-by-well basis (Figure 5/Supplementary Figure S8 for J23106). When analyzed at either a constant vanillin concentration (Figure 5A/Supplementary Figure S8A for J23106) or a constant inoculation ratio (Figure 5C/Supplementary Figure S8C for J23106) co-culture-level OD_{600} values remained similar. However, based on modeled strain-specific optical densities, the abundance of the biosensor strain within these co-cultures was highly variable, with abundance depending heavily on inoculation ratio (Figure 5B/Supplementary Figure S5B for J23106) and with increased vanillin concentration leading to a significant decrease in biosensor strain abundance (Figure 5D/Supplementary Figure S5D for J23106).

Normalizing FP fluorescence to optical density of a culture is a standard method in the application of whole-cell biosensors. Modeling of J23100 OD_{600} allows the normalization of GFP fluorescence to predicted biosensor strain abundance, enabling this relative fluorescence to be approximated in a co-culture setting. Despite a near 4-fold increase in both GFP and RFP fluorescence between cultures inoculated from 25% to 90% biosensor strain, the predicted normalized GFP levels remained relatively constant (Figure 5E/Supplementary Figure S8E for J23106). This trend was not maintained in the culture inoculated at 10% biosensor strain, as GFP and RFP fluorescence values were not discernable from background autofluorescence (Figure 4C and D/Supplementary Figure S5C and D for J23106). This indicates there is a minimum relative population density required for modeling of population dynamics in co-culture using RFP fluorescence, and likely results from inherent noisiness of fluorescence measurements. When the biosensor ratio was set at 50% or above, there was a clear trend in which increasing vanillin concentrations led to increased relative GFP fluorescence, regardless of the estimated proportions (Figure 5F/Supplementary Figure S8F for J23106). The uninduced cultures showed tight clustering of calculated normalized GFP at $0\,\mu M$, across inoculation ratios, showing decreased variability at an uninduced state. This is important in a functional screening paradigm where enzymatic activities differ broadly and any fluctuation in biosensor response above baseline could be indicative of a positive signal. The accuracy of model predictions, therefore, have implication in both the study of co-culture dynamics and the application of whole-cell biosensor screening.

3.7 Investigating co-culture dynamics in whole-cell biosensing

The relative abundance of strains in selected wells from the experiments described above were analyzed using flow cytometry to further investigate population dynamics in co-culture based on cell counts. As cell counts can distinguish variable expression at the single-cell level, this enables us to directly validate output of the model and determine variability in reporter expression as a result of co-culture format. This is essential in validating the accuracy of model-based OD_{600} predictions reported above. Samples were collected at 12, 15 and 23 h after inoculation, at three inoculation ratios (10%, 50% and 90% biosensor strain) and at two vanillin induction concentrations ($0\,\mu M$ and $320\,\mu M$). GFP and RFP expression in biosensor strains enabled them to be distinguished from EPI300-pCC1 during counting (Figure 6). As predicted by modeling of strain-specific OD_{600}, both inoculation ratio and vanillin concentration impacted relative abundance of biosensor strains and EPI300-pCC1 (Figure 6/Supplementary Figure S9 for J23106). At $0\,\mu M$ vanillin, relative abundances of strains were correlated to the inoculation ratio (Figure 6A–C/Supplementary Figure S9A–C for J23106), whereas at an induction concentration of $320\,\mu M$, relative abundances of the biosensor strain decreased over time (Figure 6D–F/Supplementary Figure S9D–F for J23106).

Although relative abundance trends related to inoculation ratio and vanillin concentration were observed in predicted OD_{600} values, measured values determined through flow cytometry-based counting deviated slightly from model predicted relative abundances in both biosensor strain J23100 (Figure 7A) and J23106 (Figure 7B). The model performed best at an inoculation ratio of 50%, whereas OD_{600} values were overpredicted at an inoculation ratio of 10% biosensor strain and underpredicted at 90% biosensor strain (Figure 7). These variations between model predicted OD_{600} values and flow cytometry-based relative abundances likely stem from the limitation of OD_{600} measurements as proxies for cell number. As a result of variable medium absorbance and refraction at low culture densities and multiple scattering events at high culture densities, the sensitivity of measurements at density extremes is decreased. This leads to over and under prediction of absolute cell abundances when using OD_{600} as a proxy (28, 29). However, this is generally considered to be an acceptable limitation in order to enable high-throughput, non-invasive approximation of cell number. Additionally, it was found that decreasing the slope of the linear model generated more accurate predictions at 50% and 90% biosensor inoculation ratios, which may enable accounting for limitations in the OD_{600} proxy.

Cumulatively, these results highlight the sensitivity of population dynamics to variations in metabolic activity within a specific strain in co-culture and the potential effect of these dynamics on the performance of functional screens. This also indicates that population dynamics can be predicted based on fluorescence levels of a marked strain in co-culture. Co-culture-level phenotypes, such as biosensor fluorescence, can then be
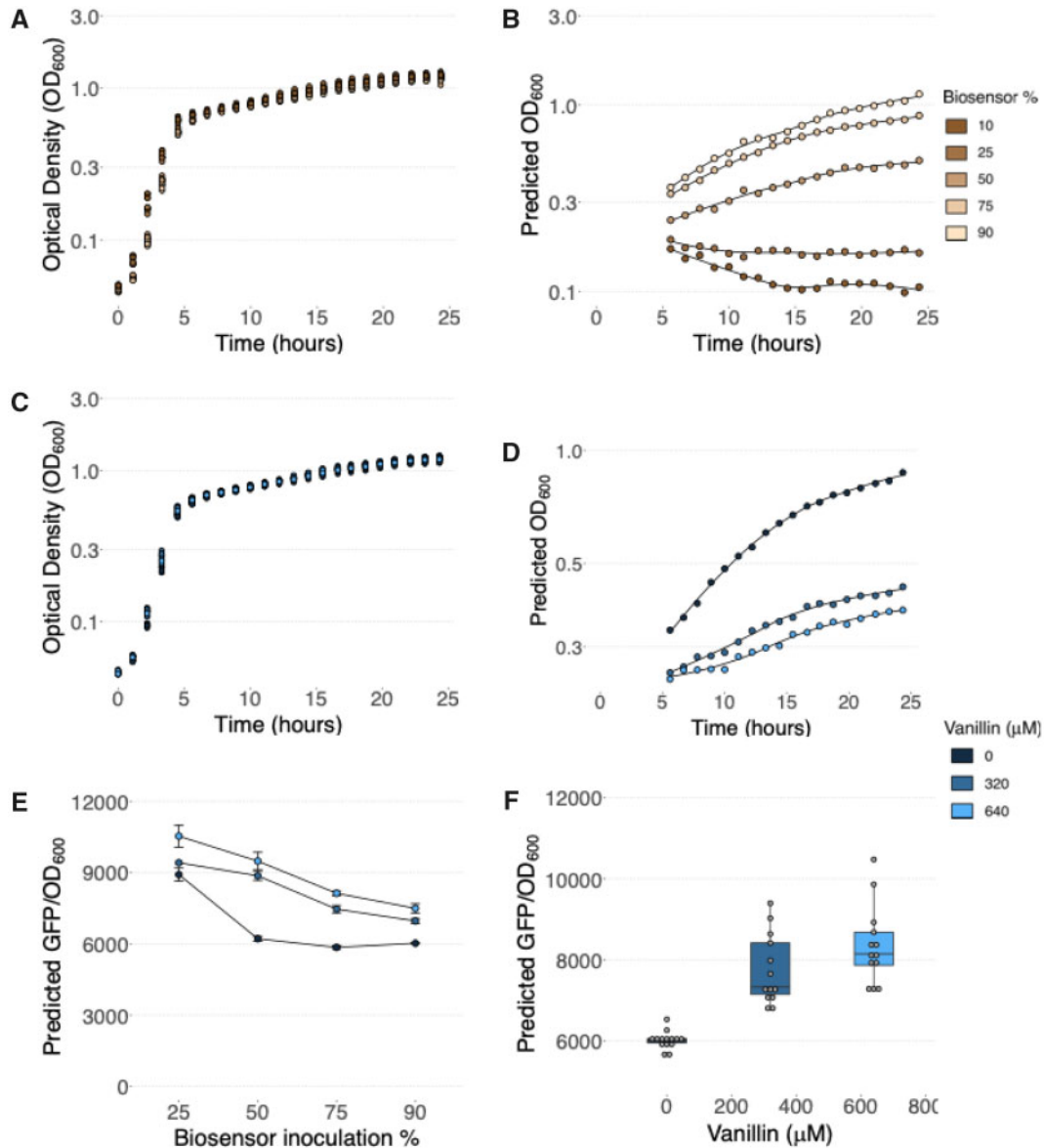
Figure 5. Calculating proportions of J23106 biosensor strain in co-culture using RFUs and predicting biosensor response through GFP normalization to calculated OD_{600}. **(A)** At a vanillin concentration of $0\,\mu M$, OD_{600} values (*Optical density*) remained relatively consistent in co-culture, regardless of biosensor inoculation ratios. **(B)** However, predicted OD_{600} of the biosensor strain (*Predicted OD_{600}*) were proportional to inoculation densities. **(C)** At a biosensor strain inoculation density of 75%, co-culture level OD_{600} values (*Optical density*) remained consistent, **(D)** whereas predicted OD_{600} values decrease with increasing vanillin concentration ($0\,\mu M$, $320\,\mu M$ and $640\,\mu M$). All values represent averages of three replicates. **(E)** GFP fluorescence was normalized to calculated biosensor-specific OD_{600} (*Predicted GFP/OD_{600}*), at increasing inoculation densities (*Biosensor inoculation %*) and vanillin concentrations. Values represent averages of three replicates. **(F)** At biosensor inoculation ratios of 50% or greater, the increase in relative GFP expression (*Predicted GFP/OD_{600}*) in response to vanillin (*Vanillin*) was consistent across ratios. There was minimal variation between calculated normalized GFP fluorescence at $0\,\mu M$ Vanillin. Points represent single samples.

normalized to predicted relative abundances to determine activity of individual marked strains.

4. Conclusions

In this article, we design, build and test an experimental high-throughput co-culture system in which to measure and model the relationship between fluorescence and cell abundance, combining CRAGE and whole-cell biosensing with a P_{emrR}-GFP monoaromatic reporter used in plate-based functional screening. We first established the CRAGE system for chromosomal engineering in the *E. coli* EPI300 screening host. This enables streamlined screening chassis engineering. Subsequently,

a series of *E. coli* EPI300 strains were engineered to constitutively express RFP and the relationship between RFP expression and optical density (OD_{600}) was determined at different stages of the EPI300 growth cycle in monoculture. Based on these observations we derived a linear equation describing the increase of normalized RFP fluorescence after entry into deceleration phase. We then applied this equation to make predictions related to biosensor strain dynamics in co-culture with EPI300 harboring the pCC1 fosmid cloning vector at different mixing ratios and inducer concentrations, and compared measured and predicted values using plate-based and flow cytometric detection methods. Induction of the biosensor lead to a significant decrease in relative abundance of the biosensor strain and a
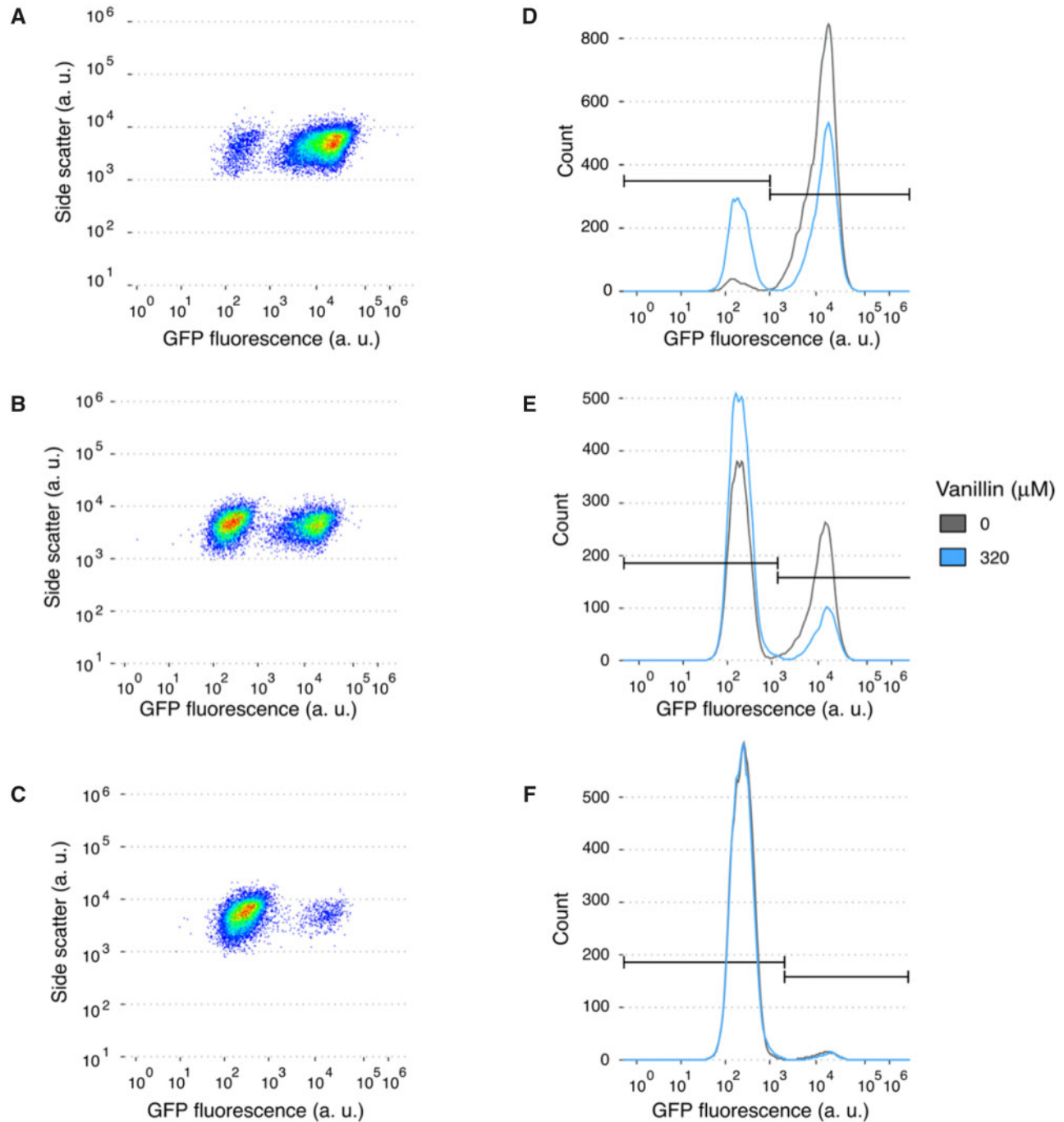
Figure 6. Determining population dynamics using flow cytometry. Proportions of strains in samples collected 15 h after inoculation are shown. At a vanillin concentration of 0 μM, relative abundances were proportional to their inoculation ratios of 90% (**A**), 50% (**B**) and 10% (**C**) J23100 biosensor strain (*Y-axis = Side scatter/X-axis = GFP fluorescence*). Plots represent events from single samples. Increased vanillin concentration from 0 μM to 320 μM led to a relative increase in EPI300-pCC1 abundance at inoculation ratios of 90% (**D**), 50% (**E**) and 10% (**E**) biosensor strain (*Y-axis = Count/X-axis = GFP fluorescence*). Histograms represent counts of two samples at either 0 μM (gray) or 320 μM (blue) vanillin.

decrease in bulk GFP fluorescence. The shift in relative strain proportions at varying biosensor induction levels has the potential to impact the interpretation of functional screening data, where analysis of plate-level fluorescence assumes consistent proportions of the biosensor strain from well to well.

In a functional screen, the metabolic burden associated with harboring any given fosmid clone will likely be variable and greater than that of harboring the empty pCC1 vector. The result will be unconstrained variation in relative abundance, dependent on both the metabolic burden of the fosmid clone and the level of biosensor response to specific activity encoded on the fosmid. This variability would also be observed in the engineering of alternative co-culture settings, such as the distribution of metabolic pathways. The current work provides a framework for determining these dynamics in high-throughput and in designing more robust plate-based screening methods.
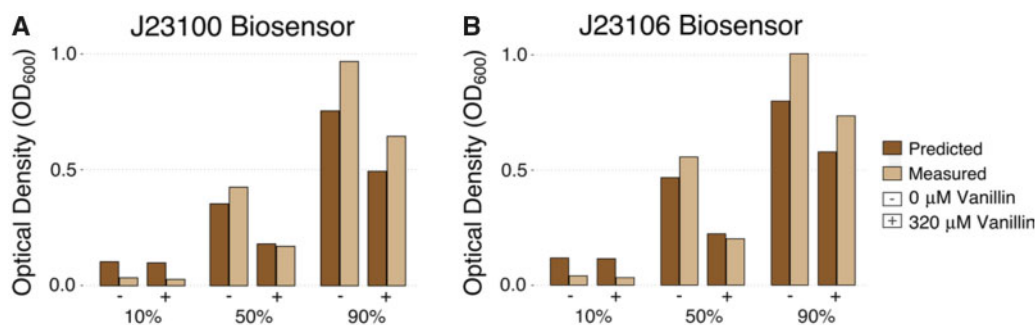
Figure 7. Model based prediction of OD_{600} values in co-culture compared to measured cell counts. Measured and predicted OD_{600} values (*Optical density*) at T_{15} are compared at two induction concentrations ($0\,\mu M$ and $320\,\mu M$ vanillin) and three inoculation proportions (10%, 50% and 90% biosensor strain). Similar trends were observed in both the J23100 (**A**) and J23106 (**B**) biosensor strains. Each bar represents either a single flow cytometry analysis or a single predicted OD_{600} value of the biosensor strain.

Representative models of the relationship between OD_{600} and FP fluorescence are likely dependent on host-strain metabolism, FP expression dynamics, medium composition and culture volume, requiring screening paradigm-specific model definition. However, we believe that observed trends would be consistent regardless of these factors, and that this type of modeling is extensible to a wide variety of strains and growth conditions. At the same time, we identified general conditions for optimal model performance. For example, hourly data collection over at least 20 h enables accurate definition of the entry into deceleration phase and that a relative biosensor abundance of at least 25% is required to detect sufficient RFP fluorescence to accurately model proportions. Moreover, the R markdown provided for this work can be used on datasets sourced from other strains with slight modification for varied input formats. Beyond the specific application of CRAGE-mediated insertion of fluorescent chromosomal markers for determining co-culture dynamics of the P_{emrR}-GFP monoaromatic reporter this work should be extensible to other biosensing and consortium engineering applications by providing novel strains for site-specific integration into the EPI300 chromosome and marked EPI300 strains expressing different levels of RFP.

Supplementary Data

Supplementary Data are available at SYNBIO Online.

Data availability

All associated data can be found in the Supplementary Materials.

Conflict of interest statement. S.J.H. is a co-founder of Koonkie Inc., a bioinformatics consulting company that designs and provides scalable algorithmic and data analytics solutions in the cloud.

References

1. Hallam,S.J. and McCutcheon,J.P. (2015) Microbes don't play solitaire: how cooperation trumps isolation in the microbial world. *Environ. Microbiol. Rep.*, 7, 392–398.
2. Hays,S.G., Patrick,W.G., Ziesack,M., Oxman,N. and Silver,P.A. (2015) Better together: engineering and application of microbial symbioses. *Curr. Opin. Biotechnol.*, 36, 40–49.
3. Goers,L., Freemont,P. and Polizzi,K.M. (2014) Co-culture systems and technologies: taking synthetic biology to the next level. *J. R. Soc. Interface*, 11, 20140065.
4. McCarty,N.S. and Ledesma-Amaro,R. (2019) Synthetic biology tools to engineer microbial communities for biotechnology. *Trends Biotechnol.*, 37, 181–197.
5. Camacho-Zaragoza,J.M., Hernández-Chávez,G., Moreno-Avitia,F., Ramírez-Iñiguez,R., Martínez,A., Bolívar,F. and Gosset,G. (2016) Engineering of a microbial coculture of *Escherichia coli* strains for the biosynthesis of resveratrol. *Microb. Cell Fact.*, 15, 163.
6. Fang,Z., Jones,J.A., Zhou,J. and Koffas,M.A.G. (2018) Engineering *Escherichia coli* co-cultures for production of curcuminoids from glucose. *Biotechnol. J.*, 13, 1700576.

7. Jones,J.A., Vernacchio,V.R., Sinkoe,A.L., Collins,S.M., Ibrahim,M.H.A., Lachance,D.M., Hahn,J. and Koffas,M.A.G. (2016) Experimental and computational optimization of an *Escherichia coli* co-culture for the efficient production of flavonoids. *Metab. Eng.*, 35, 55–63.

8. Ho,J.C.H., Pawar,S.V., Hallam,S.J. and Yadav,V.G. (2018) An improved whole-cell biosensor for the discovery of lignin-transforming enzymes in functional metagenomic screens. *ACS Synth. Biol.*, 7, 392–398.

9. Strachan,C.R., Singh,R., VanInsberghe,D., Ievdokymenko,K., Budwill,K., Mohn,W.W., Eltis,L.D. and Hallam,S.J. (2014) Metagenomic scaffolds enable combinatorial lignin transformation. *Proc. Natl. Acad. Sci. USA*, 111, 10143–10148.

10. Taupp,M., Mewis,K. and Hallam,S.J. (2011) The art and design of functional metagenomic screens. *Curr. Opin. Biotechnol.*, 22, 465–472.

11. Hug,C., Zhang,X., Guan,M., Krauss,M., Bloch,R., Schulze,T., Reinecke,T., Hollert,H. and Brack,W. (2015) Microbial reporter gene assay as a diagnostic and early warning tool for the detection and characterization of toxic pollution in surface waters. *Environ. Toxicol. Chem.*, 34, 2523–2532.

12. Lu,G.J., Farhadi,A., Mukherjee,A. and Shapiro,M.G. (2018) Proteins, air and water: reporter genes for ultrasound and magnetic resonance imaging. *Curr. Opin. Chem. Biol.*, 45, 57–63.

13. Chuang,J.S., Rivoire,O. and Leibler,S. (2009) Simpson's paradox in a synthetic microbial system. *Science*, 323, 272–275.

14. Chuang,J.S., Rivoire,O. and Leibler,S. (2010) Cooperation and Hamilton's rule in a simple synthetic microbial system. *Mol. Syst. Biol.*, 6, 398.

15. Johns,N.I., Blazejewski,T., Gomes,A.L. and Wang,H.H. (2016) Principles for designing synthetic microbial communities. *Curr. Opin. Microbiol.*, 31, 146–153.

16. Kong,W., Meldgin,D.R., Collins,J.J. and Lu,T. (2018) Designing microbial consortia with defined social interactions. *Nat. Chem. Biol.*, 14, 821–829.

17. Mee,M.T., Collins,J.J., Church,G.M. and Wang,H.H. (2014) Syntrophic exchange in synthetic microbial communities. *Proc. Natl. Acad. Sci. USA*, 111, E2149–E2156.

18. Zuñiga,C., Zaramela,L. and Zengler,K. (2017) Elucidation of complexity and prediction of interactions in microbial communities. *Microb. Biotechnol.*, 10, 1500–1522.

19. Tsoi,R., Wu,F., Zhang,C., Bewick,S., Karig,D. and You,L. (2018) Metabolic division of labor in microbial systems. *Proc. Natl. Acad. Sci. USA*, 115, 2526–2531.

20. Chen,Y., Kim,J.K., Hirning,A.J., Josi,K. and Bennett,M.R. (2015) Emergent genetic oscillations in a synthetic microbial consortium. *Science*, 349, 986–989.

21. Jawed,K., Yazdani,S.S. and Koffas,M.A.G. (2019) Advances in the development and application of microbial consortia for metabolic engineering. *Metab. Eng. Commun.*, 9, e00095.

22. Scott,S.R. and Hasty,J. (2016) Quorum sensing communication modules for microbial consortia. *ACS Synth. Biol.*, 5, 969–977.

23. Stephens,K., Pozo,M., Tsao,C.-Y., Hauk,P. and Bentley,W.E. (2019) Bacterial co-culture with cell signaling translator and growth controller modules for autonomously regulated culture composition. *Nat. Commun.*, 10, 4129.

24. Wang,Z., Wu,X., Peng,J., Hu,Y., Fang,B. and Huang,S. (2014) Artificially constructed quorum-sensing circuits are used for subtle control of bacterial population density. *PLoS One*, 9, e104578.

25. Zhang,H. and Wang,X. (2016) Modular co-culture engineering, a new approach for metabolic engineering. *Metab. Eng.*, 37, 114–121.

26. Ram,Y., Dellus-Gur,E., Bibi,M., Karkare,K., Obolski,U., Feldman,M.W., Cooper,T.F., Berman,J. and Hadany,L. (2019) Predicting microbial growth in a mixed culture from growth curve data. *Proc. Natl. Acad. Sci. USA*, 116, 14698–14707.

27. Spiegelman,D., Whissell,G. and Greer,C.W. (2005) A survey of the methods for the characterization of microbial consortia and communities. *Can. J. Microbiol.*, 51, 355–386.

28. Stevenson,K., McVey,A.F., Clark,I.B.N., Swain,P.S. and Pilizota,T. (2016) General calibration of microbial growth in microplate readers. *Sci. Rep.*, 6, 38828.

29. Dalgaard,P., Ross,T., Kamperman,L., Neumeyer,K. and McMeekin,T.A. (1994) Estimation of bacterial growth rates from turbidimetric and viable count data. *Int. J. Food Microbiol.*, 23, 391–404.

30. Myers,J.A., Curtis,B.S. and Curtis,W.R. (2013) Improving accuracy of cell and chromophore concentration measurements using optical density. *BMC Biophys.*, 6, 4–4.

31. Wang,G., Zhao,Z., Ke,J., Engel,Y., Shi,Y.-M., Robinson,D., Bingol,K., Zhang,Z., Bowen,B., Louie,K. et al. (2019) CRAGE enables rapid activation of biosynthetic gene clusters in undomesticated bacteria. *Nat. Microbiol.*, 4, 2498–2510.,

32. Dehio,C. and Meyer,M. (1997) Maintenance of broad-host-range incompatibility group P and group Q plasmids and transposition of Tn5 in *Bartonella henselae* following conjugal plasmid transfer from *Escherichia coli*. *J. Bacteriol.*, 179, 538–540.

33. Wang,B., Zhao,Z., Jabusch,L.K., Chiniquy,D.M., Ono,K., Conway,L.K., Zhang,Z., Wang,G., Robinson,D., Cheng,J.-F. et al. (2020) CRAGE-Duet facilitates modular assembly of biological systems for studying plant–microbe interactions. *ACS Synthetic Biology*, 9, 2610–2615. doi: 10.1021/acssynbio.0c00280.

34. Winterberg,K.M., Luecke,J., Bruegl,A.S. and Reznikoff,W.S. (2005) Phenotypic screening of *Escherichia coli* K-12 Tn5 insertion libraries, using whole-genome oligonucleotide microarrays. *Appl. Environ. Microbiol.*, 71, 451–459.

35. Knight,T. (2003) *Idempotent Vector Design for Standard Assembly of Biobricks*. DSpace@MIT. https://dspace.mit.edu/handle/1721.1/21168 (accessed 23 August 2020).

36. Knight,T. (2007) *Draft Standard for Biobrick Biological Parts*. OpenWetWare. http://openwetware.org/index.php?title=The_BioBricks_Foundation:BBFRFC10&oldid=262187 (accessed 23 August 2020).

37. Wery,M., Woldringh,C.L. and Rouviere-Yaniv,J. (2001) HU-GFP and DAPI co-localize on the *Escherichia coli* nucleoid. *Biochimie*, 83, 193–200.

38. Team, R.C. (2013) *R: A Language and Environment for Statistical Computing*. R Foundation for Statistical Computing. https://www.r-project.org/ (accessed 23 August 2020).

39. Wickham,H., Averick,M., Bryan,J., Chang,W., McGowan,L., François,R., Grolemund,G., Hayes,A., Henry,L., Hester,J. et al. (2019) Welcome to the Tidyverse. *J. Open Source Softw.*, 4, 1686.

40. Registry of Standard Biological Parts. (accessed 23 August 2020).

41. Mason,C.A. and Egli,T. (1993) Dynamics of microbial growth in the decelerating and stationary phase of batch culture. In: S Kjelleberg (ed). *Starvation in Bacteria*. Springer US, Boston, MA, pp. 81–102.